



**HAL**  
open science

## Complete mapping of the spin-wave spectrum in a vortex-state nanodisk

B. Taurel, T. Valet, V. V. Naletov, N. Vukadinovic, G. de Loubens, O. Klein

► **To cite this version:**

B. Taurel, T. Valet, V. V. Naletov, N. Vukadinovic, G. de Loubens, et al.. Complete mapping of the spin-wave spectrum in a vortex-state nanodisk. *Physical Review B: Condensed Matter and Materials Physics* (1998-2015), 2016, 93, pp.184427. 10.1103/PhysRevB.93.184427 . cea-01484759

**HAL Id: cea-01484759**

**<https://cea.hal.science/cea-01484759>**

Submitted on 7 Mar 2017

**HAL** is a multi-disciplinary open access archive for the deposit and dissemination of scientific research documents, whether they are published or not. The documents may come from teaching and research institutions in France or abroad, or from public or private research centers.

L'archive ouverte pluridisciplinaire **HAL**, est destinée au dépôt et à la diffusion de documents scientifiques de niveau recherche, publiés ou non, émanant des établissements d'enseignement et de recherche français ou étrangers, des laboratoires publics ou privés.

# Complete mapping of the spin-wave spectrum in vortex state nano-disk

B. Taurel,<sup>1</sup> T. Valet,<sup>2</sup> V. V. Naletov,<sup>1,3</sup> N. Vukadinovic,<sup>4</sup> G. de Loubens,<sup>5</sup> and O. Klein<sup>1</sup>

<sup>1</sup>*INAC-SPINTEC, CEA/CNRS and Univ. Grenoble Alpes, 38000 Grenoble, France*

<sup>2</sup>*SPICE Johannes Gutenberg Universität 55128 Mainz, Germany*

<sup>3</sup>*Institute of Physics, Kazan Federal University, Kazan 420008, Russian Federation*

<sup>4</sup>*Dassault Aviation, 78 quai Marcel Dassault, 92552 St-Cloud, France*

<sup>5</sup>*Service de Physique de l'État Condensé, CEA, CNRS, Université Paris-Saclay, CEA Saclay, 91191 Gif-sur-Yvette, France*

(Dated: March 2, 2016)

We report a study on the complete spin-wave spectrum inside a vortex state nano-disk. Transformation of this spectrum is continuously monitored as the nano-disk becomes gradually magnetized by a perpendicular magnetic field and encounters a second order phase transition to the uniformly magnetized state. This reveals the bijective relationship that exists between the eigen-modes in the vortex state with the ones in the saturated state. It is found that the gyrotropic mode can be continuously viewed as a uniform phase precession, which uniquely softens (its frequency vanishes) at the saturation field to transform above into the Kittel mode. By contrast the other spin-wave modes remain finite as a function of the applied field while their character is altered by level anti-crossing.

Magnetic equilibrium configurations adopting a singular topological texture such as a vortex [1], bubble [2, 3], or skyrmion [4, 5] are currently attracting a lot of attention as they allow engineering of the spin-wave (SW) spectrum with potentially improved performances for spintronic devices [6, 7]. An important feature is here the energy density of states, which overlooks inter-mode coupling. It has been found that this coupling limits the performance of spin transfer devices as it was shown in spin-orbit torque experiments [8–11]. So far the most effective topology that splits apart the bottom part of the energy spectrum is the vortex ground state. It introduces a large gap between the fundamental mode (the so-called gyrotropic mode) [12, 13] and the rest of the spectrum [14, 15]. The gyrotropic mode corresponds to a rotation of the vortex core around its equilibrium position at the disk center (the core being the small region where the magnetization points out-of-plane). Because of near translational invariance for small aspect ratio disks, it leads to a large renormalization of the associated eigen-frequency, typically found to lie below 1 GHz [12]. Never the less, it remains coupled to the higher part of the SW spectrum through an effective mass [16, 17]. Despite numerous experimental [15, 18–21] and numerical [22–25] works on the dynamics of the vortex state, a complete mapping of the SW spectrum above the gyrotropic mode has not yet been proposed. Of particular concern is the existence of hidden modes, whose odd symmetry shows no overlap with a spatially uniform averaging [26]. In parallel recent works on the sum rule invariance of the magnetic susceptibility have underlined the continuity of the spectrum independently of the magnetization texture [27]. Still, this argument of invariance has never been fully translated to a spectral point of view due to the difficulty of establishing continuity between different regions of the phase diagram.

In order to address this fundamental question, we pro-

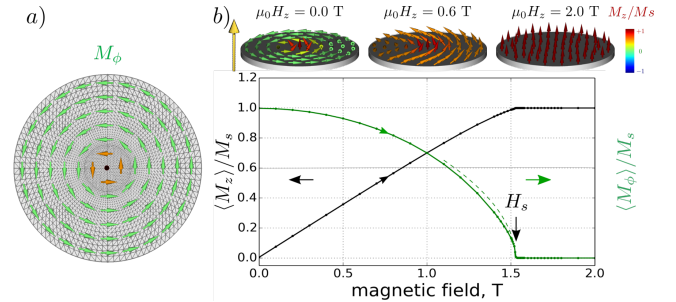


FIG. 1. (Color online) a) Micromagnetic simulations performed on a vortex-state FeV nano-disk with  $R = 100$  nm radius,  $t = 10$  nm thickness, meshed adaptively around its center. b) Variation of its reduced longitudinal (black) and azimuthal (green) magnetization along an upward perpendicular magnetization cycle (the dashed line is the behavior of the order parameter for a critical exponent = 0.5). The above schematics show the equilibrium configurations simulated for three increasing values of the perpendicular field  $H_z$ .

pose to calculate the SW spectra of a magnetic nano-disk along an upward perpendicular magnetization cycle. The perpendicular configuration allows to monitor the transformation of the SW spectrum as the magnetization texture evolves continuously from the vortex state to the uniform state, by thus avoiding any abrupt change of the equilibrium configuration [22, 28, 29]. To fully account for the spectral bijectivity, it is also important to calculate all possible eigen-vectors, including the hidden modes aforementioned. This can only be achieved by using an eigen-solver, which directly diagonalizes the linearized Landau-Lifshitz equation.

In this work, we have used the SpinFlow3D micromagnetic simulation package, a finite element simulation platform for spintronics, which has been previously validated extensively for accurate computation of eigen-modes in nano-objects [26, 30]. All micromagnetic simulations pre-

TABLE I. Parameters used in the simulation: magnetization, gyromagnetic ratio, exchange length, radius, thickness.

$\mu_0 M_s$ (T)	$\gamma$ ( $\text{rad}\cdot\text{s}^{-1}\cdot\text{T}^{-1}$ )	$\Lambda_{\text{ex}}$ (nm)	$R$ (nm)	$t$ (nm)
1.7	$1.873 \times 10^{11}$	4.3	100	10

sented below are performed on the same  $R = 100$  nm radius and 10 nm thickness disk, whose volume has been meshed adaptively around the core singularity (see mesh in Fig. 1a). The mesh-size is 1.6 nm in the central area of the disk ( $r < 25$  nm) and is increased homothetically to reach 6 nm at the periphery. The simulation is fully 3D thanks to three discretization layers along the thickness to account for the potential texture in the perpendicular direction (for a total of 8883 nodes). The magnetic parameters used in the solver are the ones of FeV listed in Table I [30]. A first numerical solver is used to calculate the equilibrium state for different values of the perpendicular magnetic field. It uses a Galerkin type finite element implementation of the very efficient projection scheme introduced in Ref. [31]. Fig. 1b shows the normal magnetization cycle produced by an upward perpendicular magnetic field swept between 0 and 2 T along  $+z$ . The initial state introduced in the simulation is a vortex configuration, with the vortex core pointing towards  $+z$ . The magnetization cycle shows an almost linear increase of the spatially averaged normal component,  $\langle M_z \rangle$ , up to the saturation field, which happens at  $\mu_0 H_s = 1.525$  T. The growth of  $M_z$  occurs mainly through the canting of the peripheral spins which gradually tilt in the perpendicular direction to form the so-called cone state [22] (see above schematic in Fig. 1b). By contrast, the averaged azimuthal component,  $\langle M_\phi \rangle$ , which can be viewed as the order parameter (see green curve in Fig. 1b), vanishes continuously at  $H_s$  indicating a second order phase transition [29].

Once the equilibrium magnetization is established at fixed values of the applied field, a second numerical solver calculates the eigen-states of the lossless linearized Landau-Lifshitz equation. It solves the corresponding generalized eigen-value problem in the vicinity of the pre-computed equilibrium state. It is solved with an iterative Arnoldi method [32] using the ARPACK library [33]. In this calculation the full complexity of the 3D micromagnetic dynamics is preserved. The solver outputs in a few minutes both the eigen-values by increasing order of energy and the associated eigen-vectors. In this work, we have restricted the output to the first 24 lowest energy modes. The results are displayed in Fig. 2. We have separated the results in two panels depending on the sense of gyration of the SW determined in reference to the core polarity.

Three remarkable features are observed in Fig. 2. The

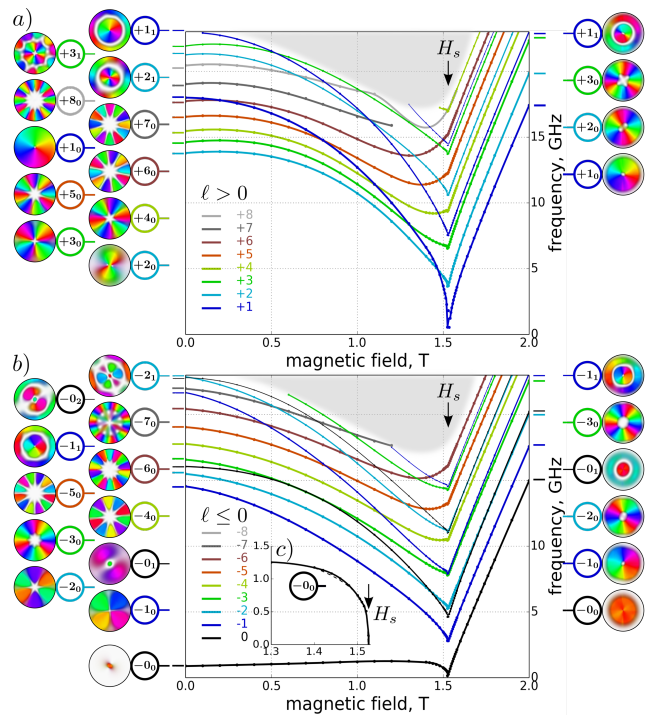


FIG. 2. (Color online) Simulated spin-wave spectra of the nano-disk as a function of the perpendicular field  $H_z$ . Modes are labeled  $(\ell_m)$ , respectively the azimuthal and radial indices. The two panels differentiate SW depending on their sense of gyration: a)  $\ell > 0$  and b)  $\ell \leq 0$ . Snapshot images of the eigen-vectors in the vortex ( $\mu_0 H_z = 0$  T) and saturated states (2 T) are shown on the left and right sides respectively (bivariate color code, where amplitude/phase = luminance/hue). c) Zoom view of the softening of the gyrotropic mode at  $H_s$  (the dashed line shows the dependence for a critical exponent = 0.3).

first one is the apparent one-to-one mapping between the eigen-modes in the vortex state and the saturated state (the discontinuities observed at the edge of the shaded area are just an artifact of the calculation constraints, where only a finite number of modes are followed). The second remarkable feature is the behavior of the lowest energy mode shown by the continuous black line in Fig. 2b. This mode is the gyrotropic mode below  $H_s$  and the Kittel mode above. Its frequency uniquely vanishes at  $H_s$ , while the eigen-modes above the gyrotropic mode always resonate at finite frequency. Such behavior seems generic to resonance modes in the presence of domain walls (see chap. 8 of [34]). The third one is that, contrary to the saturated state, where the modes evolve in parallel as a function of the applied magnetic field, in the vortex state the higher order energy levels intercept each other. It suggests that a careful analysis of the continuity of the mode character is required in the open range  $]0, H_s[$ . In the following, we shall analyze in more depths these three features.

We start with the identification of the SW spectrum.

Several works have studied the higher order modes in a vortex state nano-disks [15, 22, 24]. In particular the spatially averaged dynamic susceptibility tensor has been calculated [23]. In a recent review, we have performed such a calculation for a downward perpendicular field sweep and a positive field branch (see Fig. 4 in Ref.[29]). It was found that the in-plane component of the dynamic susceptibility varies in strength along the cycle and almost disappears close to the saturation field, leaving a blank window near  $H_s$ , which prevented the establishment of the continuity between the two phases. While this hurdle does not affect the output of SpinFlow3D shown in Fig. 2 and the continuity could be established by refining the field sweep (small dots in Fig. 2 indicate the different field values at which a spectrum has been calculated), the character of each SW mode in the vortex state remains to be assigned.

Finding the label of each eigen-state displayed in Fig. 2 requires to analyze the associated eigen-vectors. Such an analysis exists for the saturated state, where a labeling scheme has already been proposed [35]. Above  $H_s$ , the eigen-vectors form the complete set of Bessel functions [26, 36] and each eigen-state is fully described by two numbers ( $\ell_m$ ), respectively the azimuthal and radial indices indicating the winding numbers in these two directions. [Note that a third label indicating the mode index along the thickness is not necessary here [37]. For our 10 nm thin disk, one can safely consider that all modes are uniform along the thickness. Higher order perpendicular standing SW modes indeed occur outside the spectral range discussed here.] Snapshot images of the precession profiles for the normally magnetized disk are shown on the right side of Fig. 2 using a bi-variate coloring scheme: the hue codes the phase and the luminance codes the amplitude. The winding numbers are inferred from the images by counting respectively the number of times a color is complementary/repeated in the radial/azimuthal directions.

Below  $H_s$  a local magnetic texture emerges and the unit vector  $\hat{u}$  pointing in the direction of the equilibrium magnetization becomes dependent on the spatial coordinates (see Fig. 3). The norm of the magnetization being a constant of the motion, the possible eigen-vectors satisfy the local orthogonality condition to  $\hat{u}$ . Possible directions for the dynamical magnetization component are represented in Fig. 3a by a small torus attached to the magnetization vector, whose phase reference still needs to be properly defined. In the saturated state, the phase reference is naturally a fixed cartesian direction. Hence the transformation of the local frames between two positions separated by the azimuthal angle  $\phi$  occurs through a rotation of the reference frame by an angle  $+\phi$  around the disk center followed by a rotation around  $\hat{u}$  by an angle  $-\phi$ . Such transformation can be generalized to any arbitrary texture conserving the axial symmetry. For a vortex, the reference direction is shown by the small ar-

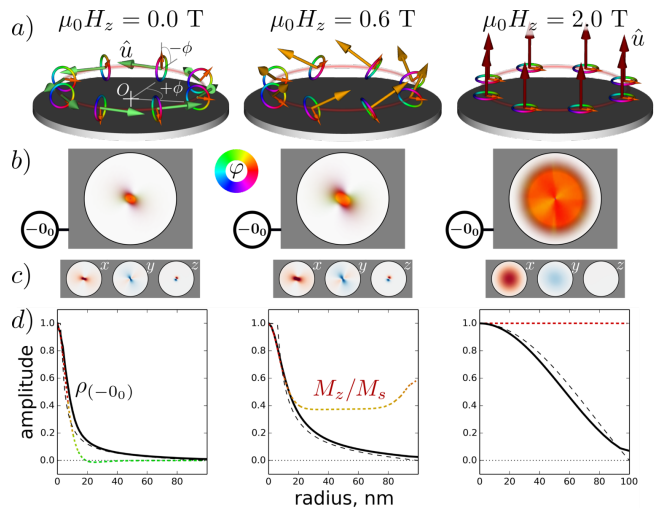


FIG. 3. (Color online) a) Dynamical magnetization vector (short arrow) in the local frame of the magnetization texture (long arrow) for the mode with a uniform phase (phase  $\varphi$  coded with the hue color wheel). b) Top view of the  $(-0_0)$  eigen-vector at  $H_z = 0.0, 0.6,$  and  $2.0$  T using either the amplitude/phase representation or c) the cartesian directions (red/blue indicates region of opposite polarity). Radial profile of the normalized rms amplitude (continuous line) compared with the analytical prediction (dashed line); the local value of the static magnetization  $M_z$  is shown for comparison using a dotted line.

row in Fig. 3a. At  $\mu_0 H_z = 0$  T the dynamical vector for a mode with a uniform phase operates a full rotation in the clockwise direction as one follows the curling magnetization anti-clockwise along the periphery. We have put on the left side of Fig. 2 the zero field snapshot images associated with each eigen-value output by the solver. The winding numbers of each image can now be inferred from the color pattern. The eigen-values are colored in Figs. 2a and 2b according to the indexation found (either a different color to dissociate SW having different  $|\ell| < 9$  index or a different line thickness to dissociate SW having different  $m < 4$  index). Extrapolating a straight line between the different points underlines the existing relationship that exists between the SW modes in the vortex and in the saturated states.

We concentrate now on the relationship that exists between the gyrotropic mode and the Kittel mode (continuous black line at the bottom of Fig. 2b). In our representation, both modes are different manifestation of the same uniform phase albeit defined over a background having different spatial texture. We have displayed in Fig. 3b a top view of the  $(-0_0)$  eigen-vector at three values of the applied field:  $\mu_0 H_z = 0, 0.6,$  and  $2$  T. We stress that the phase of the mode  $(-0_0)$ , as represented in Fig. 3b, is uniform throughout the volume, including in the core region, where  $\hat{u}$  points towards the normal direction. It is interesting to note on the representations that the spatial average of the in-plane

component of the eigen-vector is always finite, while by contrast, the averaged out-of-plane component vanishes. This even/odd symmetry can be better observed by displaying the same eigen-vectors along the cartesian directions (Fig. 3c). Thus this mode only couples to a uniform rf excitation oriented perpendicular to the core magnetization. Another important feature to notice in Fig. 2b is that, while the mode  $(-0_0)$  remains the lowest energy mode along the whole cycle, it is also the only mode that softens at  $H_s$ . The softening of SW modes at the critical fields between micromagnetic states has been investigated for the cases of elliptical elements [38, 39] and cylindrical nanodots with a large perpendicular anisotropy [3]. These critical fields correspond either to a first-order or a second-order transition. In the former case, a discontinuity in the magnetization curve occurs at the critical field and the soft mode frequency goes to zero only on one side of the transition (jump in the  $\omega(H)$  curve at the critical field). In the latter case, the magnetization curve is continuous at the critical field and the soft mode frequency goes to zero continuously on both sides of the transition. In both cases, the field dependence of the soft mode angular frequency can be described by a power law in the vicinity of the transition,  $\omega \propto |H - H_s|^\alpha$ , where  $\alpha$  is the critical exponent. For elliptical elements magnetized by a dc magnetic field applied along the minor axis, a critical exponent  $\alpha = 0.5$  has already been reported [39]. As noted above, in our case the transition between the vortex state and the saturated state is of second order. This can be evidenced by the behavior of the order parameter which vanishes continuously at  $H_s$  with a critical exponent 0.5 (see green dashed line in Fig. 1a). In our case the soft mode frequency vanishes like a power law with  $\alpha = 0.3$  (see black dashed curve in Fig. 2c). This is the same exponent as the one found for cylindrical nanodots with a perpendicular anisotropy in the presence of a dc magnetic field along the symmetry axis, for the soft mode existing at the transition between the bubble state and the saturated state [3].

Since the phase pattern of the  $(-0_0)$  mode is a conserved quantity throughout the magnetization cycle, the only quantity that is field dependent is the spatial distribution of the amplitude. It is interesting to note that top views of the precession profiles below  $H_s$  have a bow-tie shape. This feature is a direct consequence of having a finite in-plane component,  $M_\phi$ . Indeed in Fig. 3a, one can see that spins in orthogonal azimuthal direction are orthogonal to each other. Since for small aspect ratio, pointing out-of-plane is energetically defavorable compared to the in-plane direction due to depolarization effects, the precession is elliptical with the small axis in the normal direction. This ellipticity is responsible for the observed amplitude modulation in the azimuthal direction. We recall that the displayed images are snapshots: time-wise the bow-tie rotates around the disk center at the gyrotropic frequency. To account

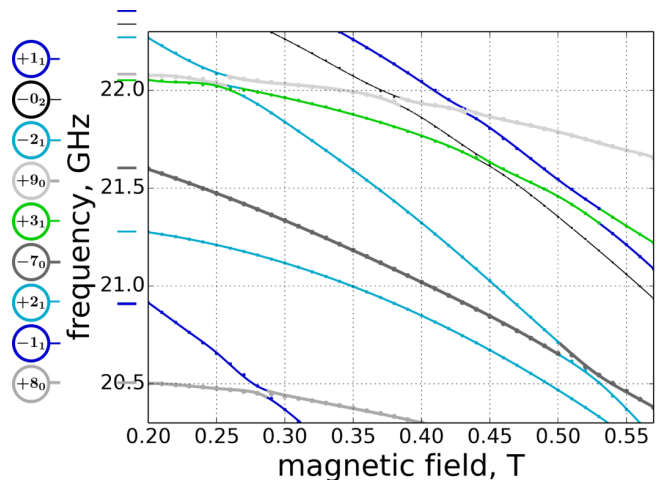


FIG. 4. (Color online) Zoom view of the level anti-crossing between SW modes of different character in the vortex state.

for this time dependence of the amplitude, we have displayed in Fig. 3d the root mean square (rms) amplitude averaged over one period. At zero field, one can notice that the precession profile  $\rho_{0_0}$  (black) extends well outside the core region (shown by the dotted profile). An analytical expression for the precession profile has been derived [40] by Guslienko *et al.* using the two vortex ansatz  $m_{0_0} \propto (1/\max(r_c, \rho) - \rho)$ , where  $r_c$  is the core radius and all quantities are expressed in reduced units of  $R$ . It is displayed by a dashed line in Fig. 3d; the predicted behavior agrees well with the simulation. Its influence zone increases with the perpendicular field. It reaches a maximum in the saturated state, where it adopts a Bessel-function shape ( $J_0$  dashed line) [41] with a node at the periphery because of dipolar pinning [42].

Although the character of the fundamental mode remains unchanged, this is not the case for the higher order SW modes, whose ranking changes along the magnetization cycle due to crossing of energy levels. As mentioned above, these crossings are responsible for the apparent discontinuities in the upper part of the spectrum. We can note that modes that bear the same  $\ell$ -index but different  $m$ -index never cross each other. The opposite is not true, in particular between pairs of opposite  $\ell$ -index. This is best seen by putting on the same plot the results shown in Fig. 2a and b. Fig. 4 is a zoom view of these combined spectra between 0.2 and 0.57 T. The zoom allows us to observe that the levels anti-cross due to inter-mode coupling. It implies that the SW character can hybridize in the vicinity of the near-degeneracy points and the SW character can be modified by performing adiabatic minor cycles around them. It implies also that at these anti-crossing the  $\ell$  and  $m$ -indices are not anymore good quantum numbers. Furthermore the strength of this coupling depends obviously on the character of the pair considered and the analysis of this underlying

selection rule remains to be done.

In summary, calculation of the eigen-states of a perpendicularly magnetized disk has allowed us to establish the spectral relationship that exists between eigen-modes in the vortex state and in the uniformly magnetized state. This provides a complete mapping of the SW spectrum above the gyrotropic mode, a particularly relevant result for the understanding of the high energy regime of vortex-state nano-objects, whose dynamics is governed by second order interaction with these new possible modes.

V. V. N. acknowledges support from the program CMIRA<sup>2</sup>Pro of the region Rhône-Alpes and from the Competitive Growth of KFU.

- 
- [1] K. Y. Guslienko, J. Nanosci. Nanotechnol. **8**, 2745 (2008).
- [2] S. Komineas, C. A. F. Vaz, J. A. C. Bland, and N. Papanicolaou, Phys. Rev. B **71**, 060405 (2005).
- [3] N. Vukadinovic and F. Boust, Phys. Rev. B **84**, 224425 (2011).
- [4] J.-V. Kim, F. Garcia-Sanchez, J. a. Sampaio, C. Moreau-Lucaire, V. Cros, and A. Fert, Phys. Rev. B **90**, 064410 (2014).
- [5] T. Schwarze, J. Waizner, M. Garst, A. Bauer, I. Stasinopoulos, H. Berger, C. Pfeiderer, and D. Grundler, Nature Mater. **14**, 478 (2015).
- [6] J. Sampaio, V. Cros, S. Rohart, A. Thiaville, and A. Fert, Nature Nanotech. **8**, 839 (2013).
- [7] A. Hamadeh, N. Locatelli, V. V. Naletov, R. Lebrun, G. de Loubens, J. Grollier, O. Klein, and V. Cros, Phys. Rev. Lett. **112**, 257201 (2014).
- [8] V. E. Demidov, S. Urazhdin, E. R. J. Edwards, M. D. Stiles, R. D. McMichael, and S. O. Demokritov, Phys. Rev. Lett. **107**, 107204 (2011).
- [9] V. Demidov, S. Urazhdin, H. Ulrichs, V. Tiberkevich, A. Slavin, D. Baither, G. Schmitz, and S. O. Demokritov, Nature Mater. **11**, 1028 (2012).
- [10] A. Hamadeh, O. d’Allivy Kelly, C. Hahn, H. Meley, R. Bernard, A. H. Molpeceres, V. V. Naletov, M. Viret, A. Anane, V. Cros, S. O. Demokritov, J. L. Prieto, M. Muñoz, G. de Loubens, and O. Klein, Phys. Rev. Lett. **113**, 197203 (2014).
- [11] M. Collet, X. de Milly, O. d’Allivy Kelly, V. Naletov, R. Bernard, P. Bortolotti, J. B. Youssef, V. Demidov, S. Demokritov, J. Prieto, M. M. noz, V. Cros, A. Anane, G. de Loubens, and O. Klein, Nature Commun. **7**, 10377 (2016).
- [12] K. Guslienko, B. Ivanov, V. Novosad, Y. Otani, H. Shima, and K. Fukamichi, J. Appl. Phys. **91**, 8037 (2002).
- [13] J. P. Park, P. Eames, D. M. Engebretson, J. Berezovsky, and P. A. Crowell, Phys. Rev. B **67**, 020403 (2003).
- [14] V. Novosad, M. Grimsditch, K. Y. Guslienko, P. Vavassori, Y. Otani, and S. D. Bader, Phys. Rev. B **66**, 052407 (2002).
- [15] M. Buess, R. Höllinger, T. Haug, K. Perzlmaier, U. Krey, D. Pescia, M. R. Scheinfein, D. Weiss, and C. H. Back, Phys. Rev. Lett. **93**, 077207 (2004).
- [16] K. Y. Guslienko, G. R. Aranda, and J. M. Gonzalez, Phys. Rev. B **81**, 014414 (2010).
- [17] K. Y. Guslienko, G. N. Kakazei, J. Ding, X. M. Liu, and A. O. Adeyeye, Sci. Rep. **5**, 13881 (2015).
- [18] J. P. Park and P. A. Crowell, Phys. Rev. Lett. **95**, 167201 (2005).
- [19] F. G. Aliev, J. F. Sierra, A. A. Awad, G. N. Kakazei, D.-S. Han, S.-K. Kim, V. Metlushko, B. Ilic, and K. Y. Guslienko, Phys. Rev. B **79**, 174433 (2009).
- [20] A. A. Awad, K. Y. Guslienko, J. F. Sierra, G. N. Kakazei, V. Metlushko, and F. G. Aliev, Appl. Phys. Lett. **96**, 012503 (2010).
- [21] K. Vogt, O. Sukhostavets, H. Schultheiss, B. Obry, P. Pirro, A. A. Serga, T. Sebastian, J. Gonzalez, K. Y. Guslienko, and B. Hillebrands, Phys. Rev. B **84**, 174401 (2011).
- [22] B. A. Ivanov and G. M. Wysin, Phys. Rev. B **65**, 134434 (2002).
- [23] F. Boust and N. Vukadinovic, Phys. Rev. B **70**, 172408 (2004).
- [24] K. Y. Guslienko, W. Scholz, R. W. Chantrell, and V. Novosad, Phys. Rev. B **71**, 144407 (2005).
- [25] H. G. Bauer, M. Sproll, C. H. Back, and G. Woltersdorf, Phys. Rev. Lett. **112**, 077201 (2014).
- [26] V. V. Naletov, G. de Loubens, G. Albuquerque, S. Borlenghi, V. Cros, G. Faini, J. Grollier, H. Hurdequint, N. Locatelli, B. Pigeau, A. N. Slavin, V. S. Tiberkevich, C. Ulysse, T. Valet, and O. Klein, Phys. Rev. B **84**, 224423 (2011).
- [27] A. Thiaville, N. Vukadinovic, and O. Acher, Phys. Rev. B **86**, 214404 (2012).
- [28] G. de Loubens, A. Riegler, B. Pigeau, F. Lochner, F. Boust, K. Y. Guslienko, H. Hurdequint, L. W. Molenkamp, G. Schmidt, A. N. Slavin, V. S. Tiberkevich, N. Vukadinovic, and O. Klein, Phys. Rev. Lett. **102**, 177602 (2009).
- [29] V. Castel, J. Ben Youssef, F. Boust, R. Weil, B. Pigeau, G. de Loubens, V. V. Naletov, O. Klein, and N. Vukadinovic, Phys. Rev. B **85**, 184419 (2012).
- [30] B. Pigeau, C. Hahn, G. de Loubens, V. V. Naletov, O. Klein, K. Mitsuzuka, D. Lacour, M. Hehn, S. Andrieu, and F. Montaigne, Phys. Rev. Lett. **109**, 247602 (2012).
- [31] W. E and X.-P. Wang, SIAM J. Numer. Anal. **38**, 1647 (2001).
- [32] M. d’Aquino, C. Serpico, G. Miano, and C. Forestiere, J. Comput. Phys. **228**, 6130 (2009).
- [33] R. Lehoucq, D. Sorensen, and C. Yang, *ARPACK Users’ Guide: Solution of Large-Scale Eigenvalue Problems with Implicitly Restarted Arnoldi Methods* (SIAM Publications, Philadelphia, 1998).
- [34] A. G. Gurevich and G. A. Melkov, *Magnetization oscillations and waves* (CRC Press, Boca Raton, 1996).
- [35] J. F. Dillon, J. Appl. Phys. **31**, 1605 (1960).
- [36] O. Klein, G. de Loubens, V. V. Naletov, F. Boust, T. Guillet, H. Hurdequint, A. Leksikov, A. N. Slavin, V. S. Tiberkevich, and N. Vukadinovic, Phys. Rev. B **78**, 144410 (2008).
- [37] X. Zhou, D. Kumar, I. S. Maksymov, M. Kostylev, and A. O. Adeyeye, Phys. Rev. B **92**, 054401 (2015).
- [38] F. Montoncello, L. Giovannini, F. Nizzoli, P. Vavassori, M. Grimsditch, T. Ono, G. Gubbiotti, S. Tacchi, and G. Carlotti, Phys. Rev. B **76**, 024426 (2007).
- [39] F. Montoncello, L. Giovannini, F. Nizzoli, P. Vavassori, and M. Grimsditch, Phys. Rev. B **77**, 214402 (2008).
- [40] K. Y. Guslienko, A. N. Slavin, V. Tiberkevich, and S.-K.

- Kim, Physical Review Letters **101**, 247203 (2008).
- [41] G. N. Kakazei, P. E. Wigen, K. Y. Guslienko, V. Novosad, A. N. Slavin, V. O. Golub, N. A. Lesnik, and Y. Otani, Appl. Phys. Lett. **85**, 443 (2004).
- [42] K. Y. Guslienko and A. N. Slavin, Phys. Rev. B **72**, 014463 (2005).